第 1 章　Analysis

1.1　Data set and event selection

The data set used in this analysis was minimum bias triggered event taken in year 2010 and year 2011 Au+Au 200 GeV collisions and central triggered date taken in year 2010 Au+Au 200 GeV collisions. For the p+p analysis, the data set was taken in year 2012 p+p 200 GeV minimum bias collision. The minimum bias trigger was defined as a coincidence in the east and west VPD detectors, and an online vertex cut was applied to select the collision happening in the center of the detector. For the central trigger, a small signal in the ZDC detectors was required as well as a large multiplicity from the barrel TOF. This trigger corresponds to 0-10% of the total hadronic cross section.

Events used in this analysis were selection by the following event selection criteria. To insure the TPC performance, events were required to have a valid reconstructed collision vertex (primary vertex, defined by primary tracks) within 30cm (for Au+Au 200 GeV collisions, Figure 1.1 (c)) and 50cm (for p+p 200 GeV collisions) of the TPC center alone the beam pipe (z direction). Figure 1.1 (b) shows correlation between TPC vertexZ and VPD vertexZ. The clean diagonal correlation band indicate the correct vertices which fire the VPDMB trigger. Random distributions could also be see in a wide region which typically indicate the vertex found be TPC is a pile-up vertex (the wrong vertex from different bunch crossing collisions). The cross like distribution in the random correlation regions is due to the online vertexZ cut in the trigger definition.To suppress the pile up events and to ensure that the selected event is firing the trigger, the difference between event vertex z-coordinate (V_z) and the V_z calculated from the VPD timing was required to be within 3cm (for Au+Au 200 GeV collisions) and 6cm (for p+p 200GeV collisions). In order to remove the events from the Au beam hitting the Beam pipe, 2cm of the vertex radius cut was also applied in the data selection. The vertex criteria is also shown in table 1.1. The events number after event selection is shown in table 1.2.

1.2　Centrality definition

The centrality in Au+Au 200 GeV collisions was defined using the uncorrected charged particle multiplicity $dN/d\eta$ within $|\eta| < 0.5$ (also called reference multiplicity). A Monte Carlo Clauber calculation was used to compared with the $dN/d\eta$

Au+Au 200 GeV	p+p 200 GeV
First primary vertex	
ranking > 0	ranking > 0
$\|Vr\| < 2cm$	
$\|Vz\| < 30cm$	$\|Vz\| < 50cm$
$\|Vz - VzVpd\| < 3cm$	$\|Vz - VzVpd\| < 6cm$

Table 1.1　vertex selection criteria.

Year	Run Type	# of events
2010	Au+Au 200 GeV MinBias	240M
	Au+Au 200 GeV Central	220M
2011	Au+Au 200 GeV MinBias	490M
2012	p+p 200 GeV MinBias	375M

Table 1.2　Number of events after event selection.

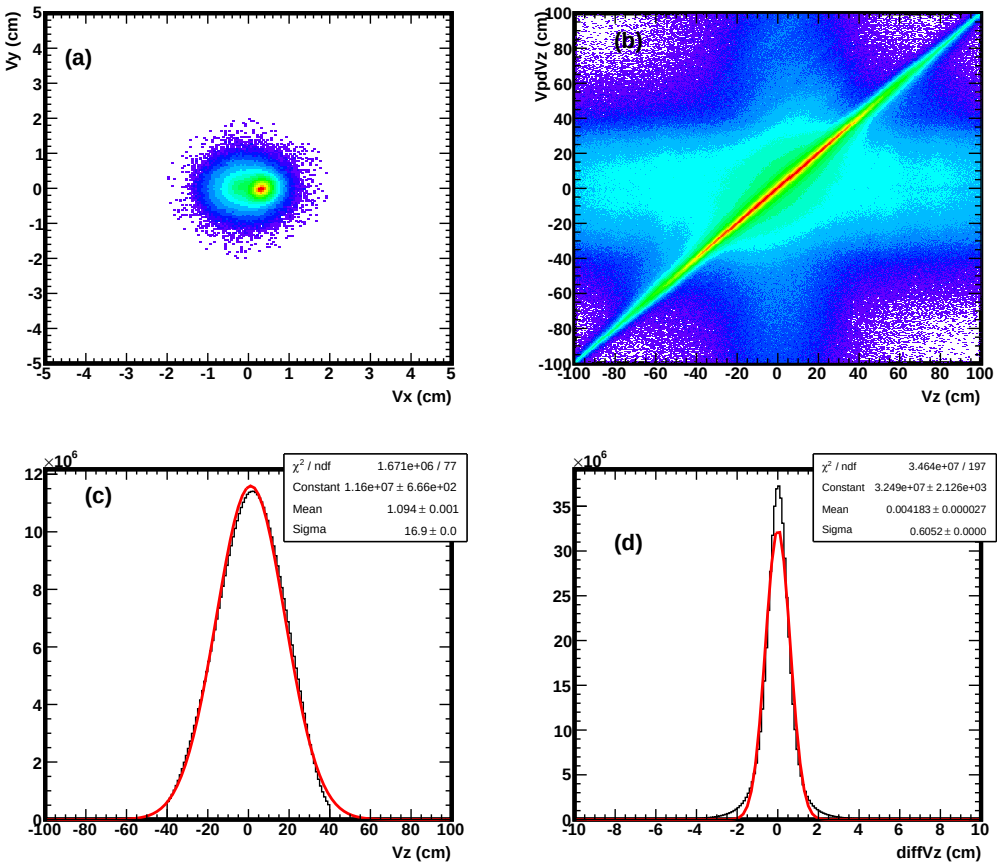

Figure 1.1　(a) TPC vertexR distribution, (b) TPC vertexZ and the VPD vertexZ correlation, (c) TPC primary vertexX distribution, (d) difference between TPC vertexZ and the VPD vertexZ in Au +Au 200 GeV minimum bias collisions.

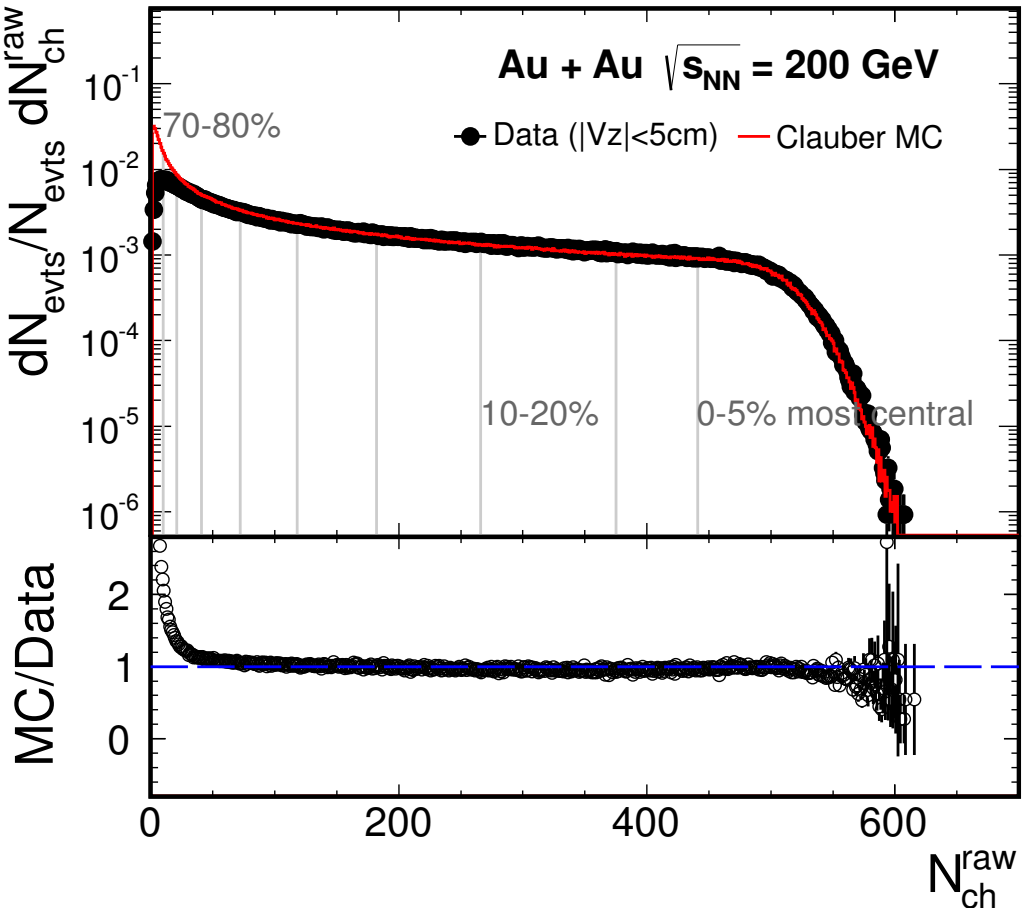

Figure 1.2 Upper Panel: Uncorrected charge particle multiplicity distribution measured within $|\eta| < 0.5$ and $|Vz| < 5cm$. The red curve represents the multiplicity distribution from MC Glauber calculation. Bottom Panel: the ratio between MC and data.

distribution from data to define centrality bins. The dependence on collision vertex Z-position and the luminosity has been also taken in account to address the efficiency and acceptance change on the measured $dN/d\eta$. Figure 1.2 shows the uncorrected $dN/d\eta$ distribution measured within $|Vz| < 5cm$ and extrapolated to zero ZDC coincidence rate for the VPDMB triggered events for Au+Au 200 GeV collision in year 2010 as well as the MC Glauber simulation. The discrepancy at the low multiplicity is because the VPD trigger efficiency starts getting lower while fewer particles are produced. The difference in low multiplicity region has been taken as a weight with the ration shown in Fig. 1.2 (bottom panel) to account for the VPD inefficiency. Finally, the centrality bins are defined according to the MC Glauder distribution to determine the cut on the measured multiplicity. Table 1.3 lists $\langle N_{part} \rangle$ and $\langle N_{bin} \rangle$ from the Glauber model simulation at $\sqrt{S_{NN}} = 200GeV$ Au+Au.

Centrality	$\langle N_{part} \rangle$	$\langle N_{bin} \rangle$
0-10%	325.5 ± 3.7	941.2 ± 26.3
10-40%	174.1 ± 10.0	391.4 ± 30.3
40-80%	41.8 ± 7.9	56.6 ± 13.7
0-80%	126.7 ± 7.7	291.9 ± 20.5

Table 1.3 Summary of centrality bins, average number of participants $\langle N_{part} \rangle$ and number of binary collisions$\langle N_{bin} \rangle$ from Monte Carlo Glauber simulation at $\sqrt{S_{NN}} = 200GeV$ Au+Au collision.

1.3 Track selection and electron identification

1.3.1 Track selection

Electron (including positrons if not specified) candidates are selected from good tracks satisfied the flowing selection:

1. number of fit points (*nHitsFit*) in the TPC greater than 20 (maximum 45) to ensure good tracking quality and momentum resolution;

2. the ratio of number of fit points over number of possible fit points in TPC greater than 0.52 to avoid split tracks in the TPC;

3. distance of closet approach (*dca*) to the primary vertex less then 1 cm to make sure selected tracks are from the primary collision;

4. number of *dE/dx* points used for calculation average *dE/dx* greater than 16 to ensure good *dE/dx* resolution.

5. with a valid matching to a TOF hit and projected position on TOF module with the sensitive readout volume.

Table 1.4 left part lists the detailed track quality cut.

1.3.2 Electron identification

In additional of track detection, momentum determination, TPC also provide particle identification for charged particles by measuring their ionization energy loss (*dE/dx*) in the TPC gas. Usually, a normalized *dE/dx* (also called $n\sigma$) is used, which is defined:

$$n\sigma_e = \frac{1}{R_{dE/dx}} ln \frac{\langle dE/dx \rangle^{Mea}}{\langle dE/dx \rangle_e^{Bichsel}} \tag{1.1}$$

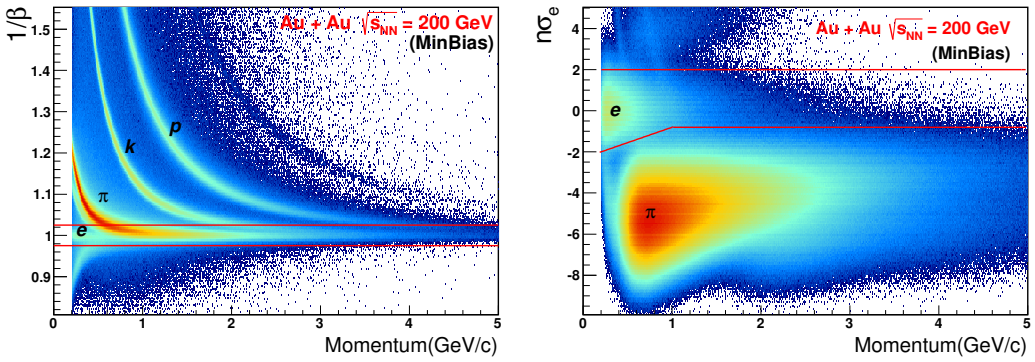

Figure 1.3 Left panel: inverse velocity $1/\beta$ vs momentum distribution in 200GeV Au+Au collisions. Right panel: $n\sigma_e$ distribution as a function of momentum after TOF velocity cut $|1/\beta - 1| < 0.025$ in 200GeV Au+Au collisions. The red lines in both panel show the PID cuts.

in the formula 1.1: $R_{dE/dx}$ is the *dE/dx* resolution, *Mea* and *Bichsel* are measured value and theoretical value. $n\sigma_e$ follows a standard gaussian distribution.

With TPC only, however, it is difficult to separate electron from hadrons because the electron band crosses with hadron bands in higher momentum. With the flight timing information measured by TOF and the track path-length measured from TPC, we can calculate the velocity (β). Due to the very small electron mass, electron can be separated from the slow hadron by the velocity cut. Combining the velocity (β) information from TOF and energy loss(*dE/dx*) from TPC, electron can be identified up to momentum ~3GeV/c. Figure 1.3 left panel shows the inverse velocity distribution as a function of momentum, while the $n\sigma_e$ vs momentum distribution after TOF velocity cut is shown in right panel. The detailed eID cuts are listed in Table 1.4.

Track quality cuts		PID cuts	
dca	<1cm	p_T	> 0.2GeV/c
nHitsFit	>= 20	$n\sigma_e, p < 1.0GeV/c$	$1.5 \times (p-1) - 0.8 \sim 2.0$
nHitsFit/nHitsPoss	>=0.52	$n\sigma_e, p > 1.0GeV/c$	$-0.8 \sim 2.0$
ndEdxFit	>=16	TOF $1/\beta$	$\|1 - 1/\beta\| < 0.025$ (Au+Au)
η	+/- 1		$\|1 - 1/\beta\| < 0.03$ (p+p)
		TOF yLocal	$\|yLocal\| < 1.8cm$

Table 1.4 Electron selection criteria

1.3.3 Hadron contamination and electron purity

From Fig 1.3 right panel, even after the TOF cut, the slow hadron bands can still be seen in $n\sigma_e$ vs momentum. We selected pure hadron (π, k and p) sample by a very

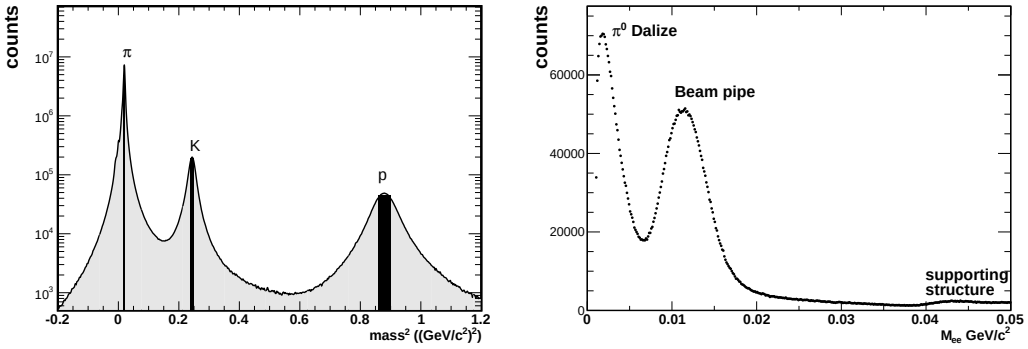

Figure 1.4 Left panel: Hadron sample selected by TOF. Right panel: pure electron sample from π^0 Daliza decay and photonic conversion.

Au+Au 200GeV	MinBias	$\sim 0.946 \pm 0.024$
	Cenrtral	$\sim 0.921 \pm 0.025$
p+p 200GeV	MinBias	$\sim 0.980 \pm 0.040$

Table 1.5 Electron purity for different data samples.

tight m^2 cut provided by TOF (shown in Fig 1.4 left panel). The pure electron sample was from photonic conversion and π^0 Dalitz decay (Fig 1.4 (right)). Gaussian functions were used to parameterize the $n\sigma_e$ distribution from the pure sample for different particle species. Then, the hadron contamination and electron purity were studied by multi-gaussian fit to the $n\sigma_e$ distribution in differential momentum bins to obtain the yields for different particles. The mean and σ were fixed in the fit respecting to the value obtained from the pure sample. Figure 1.5 picks up the fit result in momentum bin [0.6, 0.64) GeV/c as an example. The fit also included the merged π component which is from that the merging of two closed π tracks, and has a doubled *dE/dx* value compared to a normal π track. In some momentum regions, the electron band crosses with the hadron bands, where the multi-gaussian fit may not be reliable. In this analysis, exponential functions were used to extrapolate the particle yields into the cross region (Figure 1.7 (left), and the uncertainties from the exponential fit were taken into account as systematic uncertainty. Figure 1.7 right panel shows the electron purity for Au+Au 200GeV minimum bias data taken in year 2011. Table 1.5 lists electron purity for the data set used in this analysis.

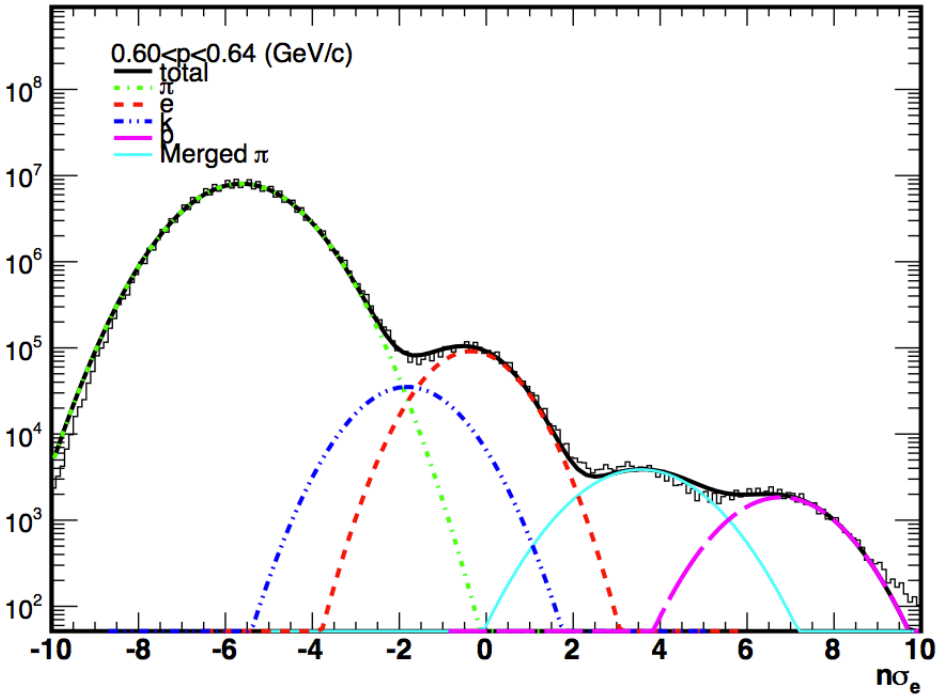

Figure 1.5　A multi-gaussian fit in momentum bin [0.6, 0.64) (GeV/c) in Au+Au 200GeV minimum bias collisions.

1.4　Pair reconstruction and background

The dielectron pairs (foreground, also marked as *unlike-sign pairs*) were reconstructed by randomly combining electron and position from the high purity electron (position) sample from the same event. The invariant mass of di-electron pairs M_{ee} were calculated as :

$$M_{ee} = \sqrt{(E_+ + E_-)^2 - (\vec{p_+} + \vec{p_-})^2} \tag{1.2}$$

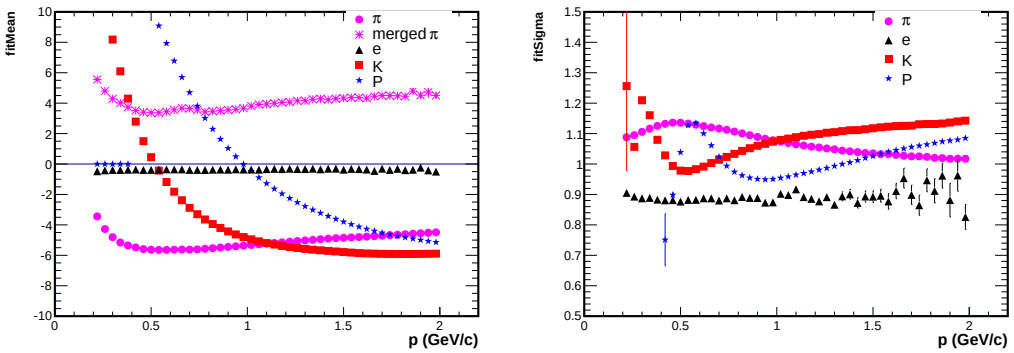

Figure 1.6　Mean (left) and sigma (right) of the gaussian distribution as a function of momentum from pure samples for different particle species in Au+Au 200GeV minimum bias collisions.

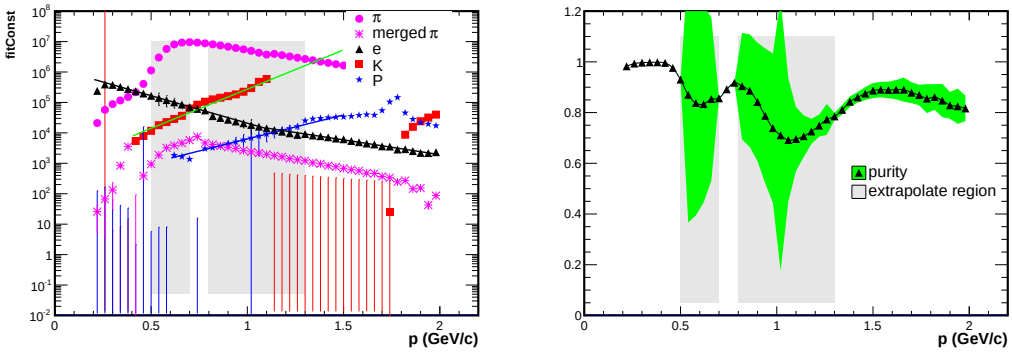

Figure 1.7 (left) Yields for different particle species from multi-gaussian fit as a function of momentum. The grey area show the cross region. And the solid lines depict the exponential fits to extrapolate the yields in the cross region. (right) Electron purity as a function of momentum, the green band represents he uncertainty from the extrapolation and the multi-gaussian fits.

where $E_{\pm} = \sqrt{(\vec{p_{\pm}})^2 + m_e^2}$, $m_e = 0.511 MeV/c$, and $\vec{p_{\pm}}$ is the momentum of electron (positron) which was measured by TPC. The candidate tracks were required to satisfy cut: $p_T > 0.2 GeV/c$ and $|\eta| < 1$ to fit into the acceptance of STAR detector, while the dielectron pairs were constructed in mid-rapidity ($|y_{ee}| < 1$). Unlike-sign pairs include the dielectron signal and background, where the signal is defined by dielectron pairs from hadron decay, and QGP/media contribution which is what we are interested . On the other hand, the background includes the following source:

1. Combinatorial background: background come from randomly pairing, which is uncorrelated.

2. Correlated background, which is the case that two partner tracks come from different parents but from the same source. E.G, $\pi^0 \to \gamma + e^+e^-$, then γ converts into another e^+e^- pair, when randomly combination, it is possible to pick one track from π^0 decay and another from the converted photon. There is also contribution from Jet, e.g electrons and positrons from same Jet or back to back Jet. In this case, the final state particles are correlated, which is mainly contributed in high momentum and high mass region. In additional, the hadron contamination also has small contribution, e.g π, p from Λ decay are misidentified by electrons. This contribution was considered as systematic uncertainty, and will be discussed in following section.

3. Photon conversion. The invariant mass of dielectron pairs from real photon conversion should be 0. However, due to the primary track reconstruction algorithm, the momentum of these electrons from conversion which happened away from the

primary vertex are biased, which lead to a finite pair invariant mass. This kind of background mainly contributes in very low mass region ($M_{ee} < 0.2GeV/c^2$). It will be discussed in detail in follow section.

In this analysis, we adopted two methods to reproduce the background.

1.4.1 Like-sign method

The Like-sign method is used to calculate contributions of uncorrelated and correlated background at the same time and serves as a standard of the background to justify the background distribution. In this analysis, we constructed like-sign background by randomly combining same charge pairs N_{++} , N_{--} from the same event. We used the geometric mean of the like-sign pairs $2\sqrt{N_{++} \times N_{--}}$, because it is demonstrated in this paper (cited) that when the e^+ and e^- are produced in statistically independent pairs, the geometric mean fully describes the background in the unlike-sign pair foreground distribution.

The TPC detector has de-active zones, (e.g the gap between TPC sectors), and in magnet field, different charged particles are bended into opposite direction. Therefore, the acceptance of different charged particle is different. Figure 1.8 shows the transverse momentum (p_T) vs azimuthal angle (ϕ) distribution of negative tracks and positive tracks in magnet field. The white bands show the de-active regions of TPC. In Figure 1.8, it can be clearly seen that the acceptance effect is different for negative and positive charged tracks. So due to the acceptance effect, the acceptance of unlike-sign pairs and like-sign pairs are different (Fig 1.9).

To address this difference, mixed event method was used in this analysis. Due to it does not include correlated pairs, mixed event method can be used to study the detector acceptance effect. The like-sign background was calculated by formula 1.3, and the acceptance correction factor also defined there. The p_T dependence was also considered by applying a 2D (mass vs p_T) acceptance factor correction, and the difference between 2D and 1D was included in systematic uncertainty. Figure 1.10 shows acceptance correction factor as function of M_{ee} in 200 GeV Au+Au and p+p minimum bias collisions.

$$
\begin{aligned}
N_{likesign}(M_{ee}, p_T) &= 2\sqrt{N_{++}(M_{ee}, p_T) \times N_{--}(M_{ee}, p_T)} \cdot F_{acc}(M_{ee}, p_T) \\
F_{acc}(M_{ee}, p_T) &= \frac{N^{Mix}_{+-}(M_{ee}, p_T)}{2\sqrt{N^{Mix}_{++}(M_{ee}, p_T) \times N^{Mix}_{--}(M_{ee}, p_T)}}
\end{aligned}
\tag{1.3}
$$

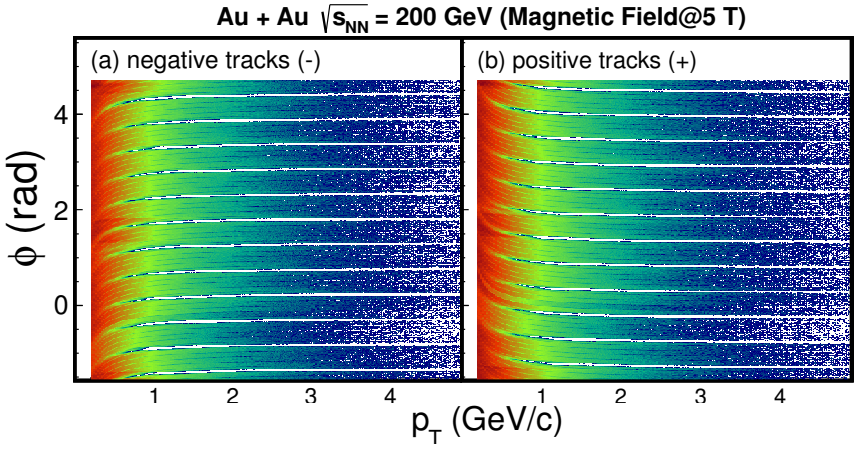

Figure 1.8　p_T vs ϕ distribution for negative tracks (a) and positive tracks (b) in magnet field.

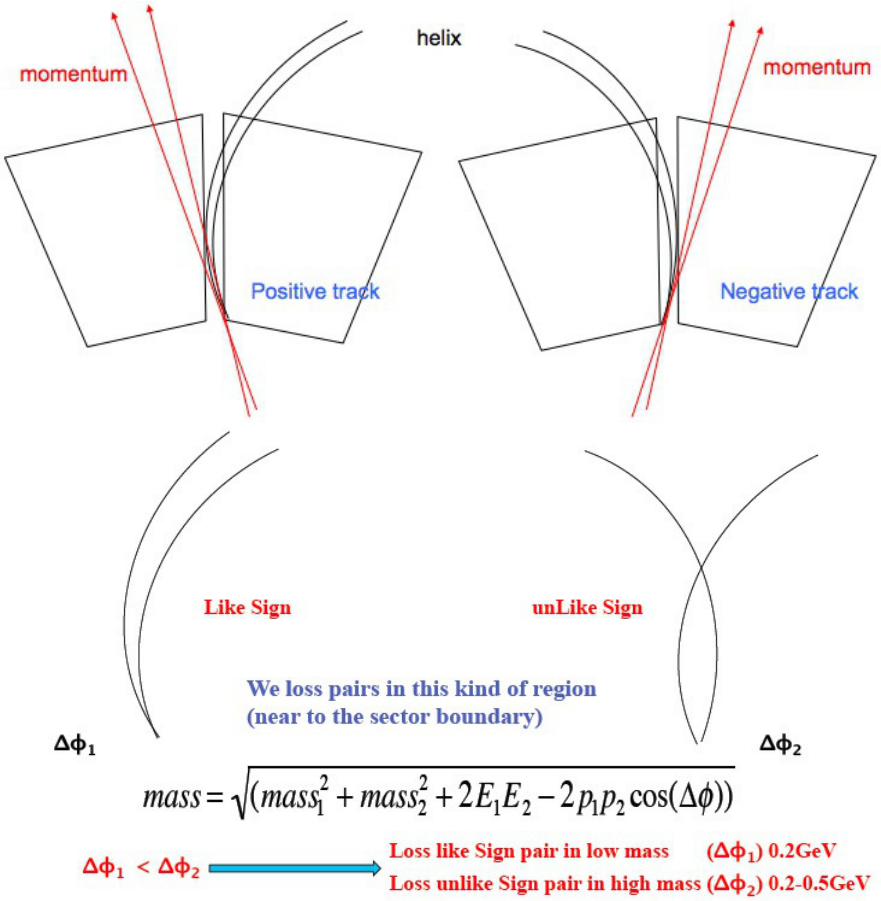

Figure 1.9　A cartoon shows the acceptance difference between unlike-sign pairs and like-sign pairs.

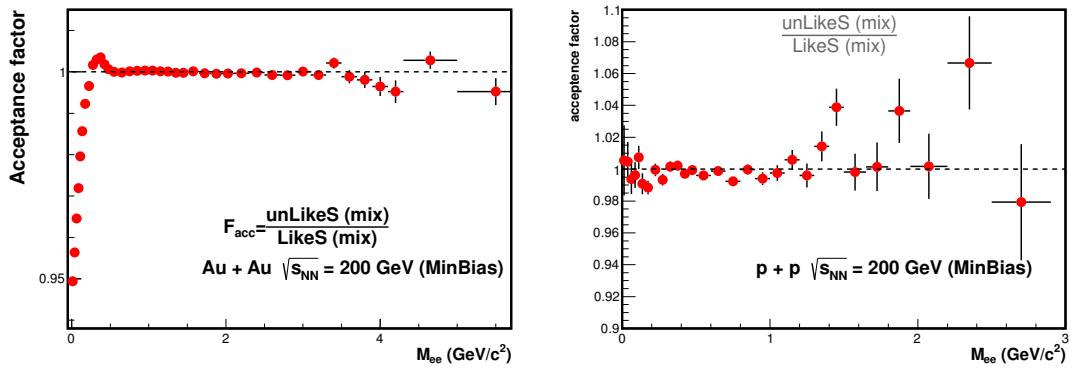

Figure 1.10 (left) Acceptance correction factor in Au+Au 200 GeV collision. (right) Acceptance correction factor in p+p 200GeV collision.

1.4.2 Mixed event method

Like-sign method as mentioned in section 3.4.1 can fully reproduce combinatorial background and correlated background. However, the like-sign background is leak of statistics. In this analysis, the like-sign background was used in low mass region where we have better statistics. For higher mass region, event mixing technique was used to achieve better statistical accuracy.

Mixed event background is reproduced by mixing electron candidate tracks from different event. Since the two tracks are uncorrelated, mixed event method is only able to reconstruct combinatorial background. To ensure events mixed together have similar structure, we classified event sample according magnet, centrality, Vz and event plane, and split it into $Magnet \times Centrality \times EventPlane \times Vz = 2 \times 9 \times 12 \times 10$ event pools. Each event pool holds 50 (100 for p+p data) events at maximum, when the number of events in the event pool reach limitation, one event is randomly dropped to make space for the new coming events. Dr. Jie Zhao did very detailed study about the number of event pools and event buffer effect on mixed event background in (cite). Here we chosen the number of event pools and event buffer respecting to his study.

The mixed event background should be normalized to the same amplitude of like-sign background, since the like-sign background can fully reproduce the real background. The formula is used to calculate the normalization factor:

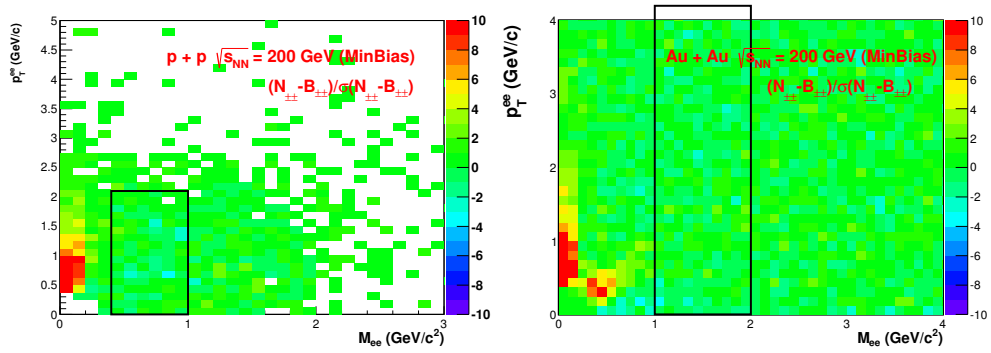

Figure 1.11 The difference between like-sign background and mixed event background divided by its standard deviation $(N_{likesign} - N^{Mix}_{likesign})/\sigma(N_{likesign} - N^{Mix}_{likesign})$ in p+p collision (left) and in Au+Au collision (right). the black box represent the chosen normalization region: $0.5 < M_{ee} < 1GeV/c^2$, $0 < p_T^{ee} < 2GeV/c$ for p+p data and $1 < M_{ee} < 2GeV/c^2$ for Au+Au data.

$$
\begin{aligned}
A_{\pm} &= \frac{\int_{N.R} N_{\pm\pm}(M,p_T)dMdp_T}{\int_{N.R} N^{Mix}_{\pm\pm}(M,p_T)dMdp_T} \\
B_{\pm\pm} &= \int_0^{\infty} A_{\pm} N^{Mix}_{\pm\pm}(M,p_T)dMdp_T \\
N^{Norm}_{Mix}(M,p_T) &= \frac{2\sqrt{B_{++}B_{--}}}{\int_0^{\infty} N^{Mix}_{+-}(M,p_T)dMdp_T} N^{Mix}_{+-}(M,p_T)
\end{aligned}
\tag{1.4}
$$

N.R represents the normalization region. The statistical uncertainty of the normalization factor is included into the total statistical uncertainty.

However, since the mixed event method can not reconstruct correlated background, the shape of mixed event background is expected to be different with the like-sign background. The normalization region was chosen as the flat region in $(N_{likesign} - N^{Mix}_{likesign})/\sigma(N_{likesign} - N^{Mix}_{likesign})$ which is shown in Fig 1.11. To take into account the difference between the like-sign and mixed event background, we used function 1.5 to fit the ratio of like-sign over mixed event background (Fig 1.12), and subtracted it in additional as *residue* of the correlated component from the foreground. The 68% confidence level of the fit was taken into accounted as systematic uncertainty.

$$
f(M_{ee}) = 1 + exp((M_{ee} - a)/b) \qquad a, b \sim free\,parameters \tag{1.5}
$$

1.4.3　Photon conversion

Photon conversion is that photon hit material of detectors and convert to e^+e^- pairs. When reconstructed unlike-sign foreground, it has contribution to the very low mass region ($M_{ee} < 0.2GeV/c^2$). Therefore, it must be subtracted from the signal. The pair

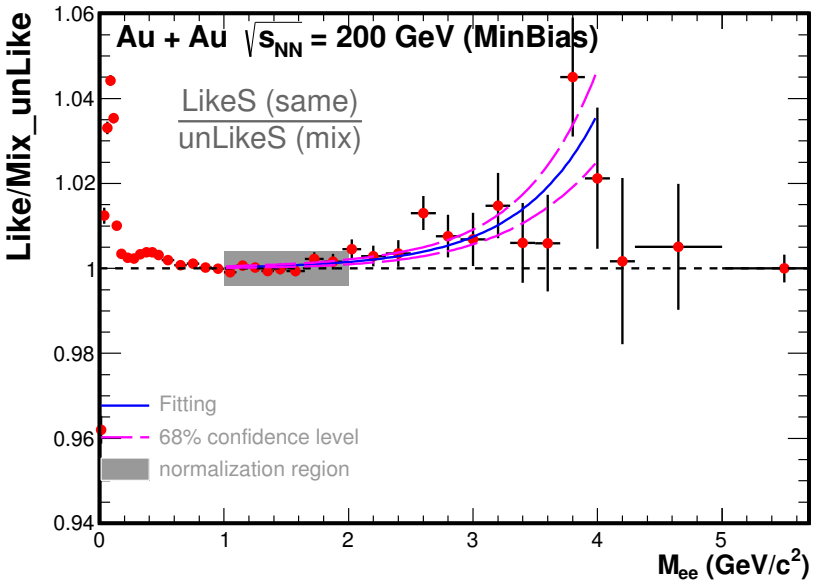

Figure 1.12 The distribution of like-sign over mixed event background ratio as a function of M_{ee}. The solid line depicts a fit to the raise about 1 GeV/c^2, while the dashed line shows 68% confidence level of the fit.

mass from photon conversion pairs should be 0. However, momentum of electron tracks from conversion vertex away from primary vertex is biased which lead to a finite pair invariant mass, because the procedure of reconstruction primary tracks also included the primary vertex as a fit point.

In this analysis, we used ϕ_V cut method which is similar to the method used by PHENIX (cite). Considering the zero opening angle of di-electron pairs from photon conversion, electron is bended inside the plate perpendicular to magnet direction. Therefore, ϕ_V is defined as formula 1.6, where $\vec{p}_+$, $\vec{p}_-$ are the momentum of e^+ and e^-, respectively, $\hat{z}$ is the direction of magnet.

$$\begin{aligned} \hat{\mu} &= \frac{\vec{p}_+ + \vec{p}_-}{|\vec{p}_+ + \vec{p}_-|}\,,\ \hat{\nu} = \vec{p}_+ \times \vec{p}_- \\ \hat{\omega} &= \hat{\mu} \times \hat{\nu}\,,\ \hat{\omega}_c = \hat{\mu} \times \hat{z} \\ \cos\phi_V &= \hat{\omega} \cdot \hat{\omega}_c \end{aligned} \tag{1.6}$$

ϕ_V should be zero, if the di-electron pair is originated from photon conversions. While, there is no preferred orientation for combinatorial pairs, and very weak dependence for di-electron pairs from hadron decays. A Geant simulation was done to study the distribution of ϕ_V vs mass (Fig 1.13(left) (cite)). And the cut used in this analysis is

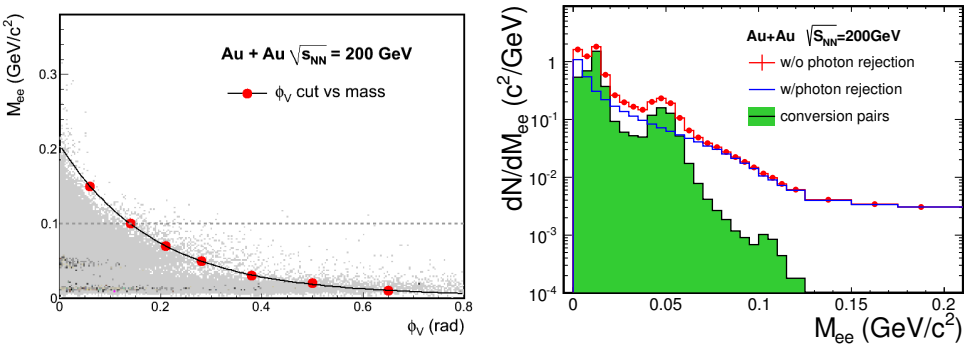

Figure 1.13 (left) ϕ_V *vs mass* distribution from Geant simulation, the solid line depicts the cut. (right) Di-electron mass spectra with photon rejection, without photon rejection and conversion pairs distribution from 200GeV Au+Au data. The conversion peaks from left to right are came from conversion happened at beam pipe (r~4cm), TPC supporting structure (r~20cm) and TPC inner field cage (r~46cm) , respectively.

shown as the red solid line (cite). The conversion pairs were directly removed by this cut. This cut was only applied in very low mass ($M_{ee} < 0.2GeV/c^2$). Simulation shows ~95% conversion pairs are removed by this cut.

1.4.4 Centrality and p_T^{ee} dependence

In this analysis, for the Au+Au collision data, we also measured the di-electron mass spectra in different centrality bins and p_T^{ee} regions. The centrality and p_T^{ee} dependence of acceptance factor and correlated residue were also studied. Figure 1.14 shows the acceptance factor correction (acceptance difference between unlike-sign pairs and like-sign pairs) in different centrality and p_T bins. The acceptance factor shows a clear p_T dependence. It is because the bending effect in magnetic field is weaker for charged particles with higher p_T . The acceptance between positive and negative charged tracks is smaller at higher p_T. The correlation background residue distribution were also studied by using function 1.5 to fit the like-sign over mixed event background ratio in different centrality and p_T regions (Fig 1.15).

1.4.5 Di-electron signal

The follow tactics was used to subtract the background from the unlike-sign foregound:

- Considering the correlated component, we subtracted the like-sign background with a acceptance factor correction in mass region ($M_{ee} < M_{th}$, where $M_{th} = 1GeV/c^2$ for Au+Au collision, and $M_{th} = 0.4GeV/c^2$ for p+p collision), where the like-sign background has enough statistics.

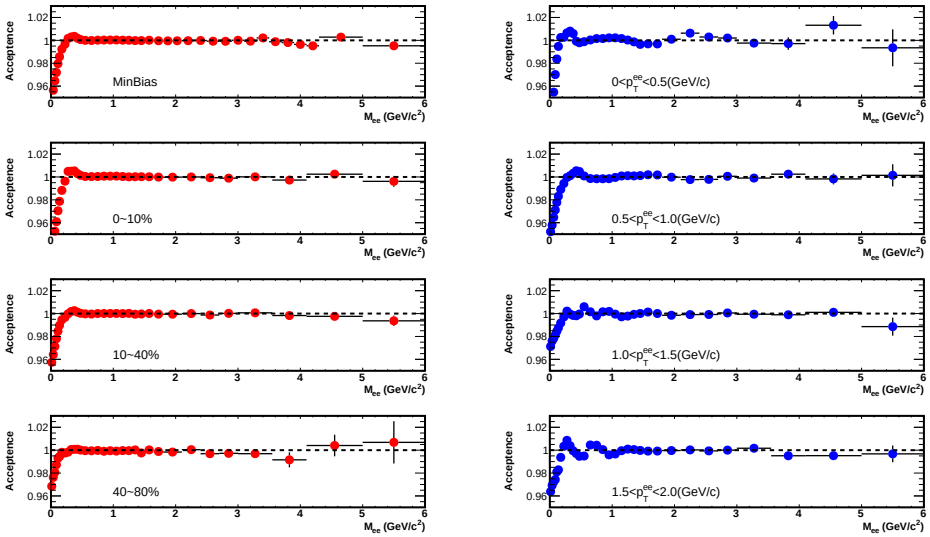

Figure 1.14 Acceptance factor in different centrality (left) and p_T (right) bins, for 200 GeV Au +Au collision data.

- For the mass region above M_{th}, the normalized mixed event background was subtracted. And we subtracted the correlated component (Jet contribution) by fitting the ratio of like-sign over mixed event background (formula 1.5).

After the background subtraction, we got the raw di-electron spectra without efficiency correction. Figure 1.16 shows di-electron signal, foreground and background, as well as the signal over background ratio.

1.5 Efficiency and acceptance correction

The di-electron raw signal yields was corrected for efficiency within STAR acceptance of $|y_{ee}| < 1$, $|\eta_e| < 1$ and $p_T^e < 0.2GeV/c$. To calculate the efficiency, we first need single electron efficiency which can be separated into two parts: detector efficiency and PID efficiency. Then Monte Carlo method is used to evolved the single efficiency into pair efficiency. We will discuss it step by step, in the following sections.

1.5.1 Single electron efficiency

The single electron efficiency in this analysis included the TPC tracking efficiency (ε_{TPC}), TOF matching efficiency (ε_{TOF}) and electron identification efficiency (ε_{PID}) as formula 1.7.

$$\varepsilon_{single} = \varepsilon_{TPC} \times \varepsilon_{TOF} \times \varepsilon_{PID} \tag{1.7}$$

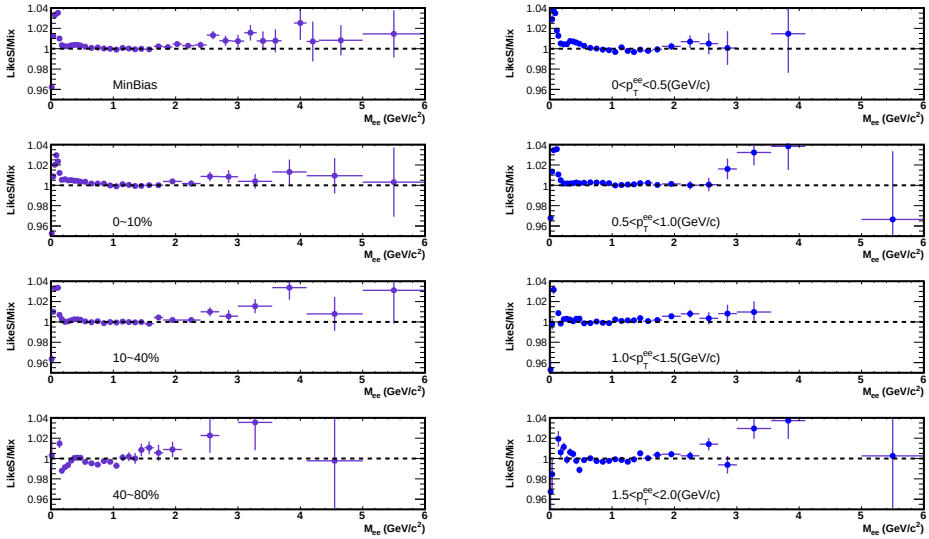

Figure 1.15 Like-sign over mixed event background ratio in different centrality (right) and p_T (left) bins, for 200 GeV Au+Au collision data.

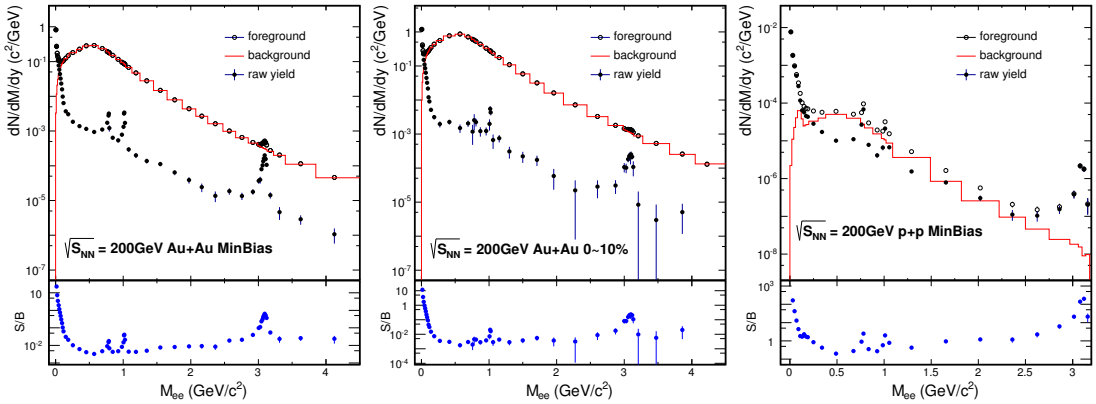

Figure 1.16 Unlike-sign foreground, background, raw di-electron spectra and signal over background ratio for Au+Au minimum bias (left), central (middle) collision and p+p minimum bias (collision).

The TPC tracking efficiency includes the track reconstruction efficiency and the TPC acceptance loss. Also the track quality cut (nHitFits, dca) efficiency are also combined into TPC tracking efficiency. The TPC tracking efficiency was obtained via the standard STAR embedding process. Monte Carlo (MC) electron tracks were generated within a certain phase space definition. The embedding tracks were sent into the GSTAR simulator and passed through STAR detector geometry corresponding to the data set and detector response simulator (TRS, TPC Response Simulator) to simulate the detector signal. Then, the MC tracks were mixed with the real data which we called embedding sample here. The embedding sample were reconstructed by the same offline reconstruction chain used to produce real data. The tracking efficiency is defined by number of reconstructed MC tracks which is satisfied the track quality cut divided by

number of input MC tracks, also see formula 1.8.

$$\varepsilon_{TPC} = \frac{N_{rc}(nHitsFit \geqslant 20,\ dca < 1cm)}{N_{Mc}} \tag{1.8}$$

To qualify whether the embedding sample can reproduce the real data, we compared several track parameters from embedding sample with those from the pure electron sample selected by photon conversion and π^0 Daliza decay. The difference was included into the systematic uncertainty.